RANS and DES Turbulence Model Predictions on the M219 Cavity at M = 0.85

Richard Allen, Fred Mendonça
CD adapco Group, London, UK

David Kirkham
BAE SYSTEMS, Farnborough, UK

Author for correspondence: rallen@uk.cd-adapco.com

ABSTRACT TITLE

Two rectangular cavity configurations, with and without bay doors, at Mach 0.85 are investigated with the objective of assessing the ability of 3D CFD with advanced turbulence modelling to predict narrowband and broadband flow noise. A non-linear, two-equation, eddy-viscosity model run in unsteady mode (URANS) is compared with Detached Eddy Simulation (DES) on a cavity with a L/D ratio of 5. In a thorough evaluation, comparisons are made between DES variants published in the literature, namely Spalart-Allmaras, k-ε and k-ω-SST. We also assess the effect on the noise spectra of using different CFD prediction time-samples of approximately 100 flow passes compared with 250 flow passes. Detailed experimental data for both cavity configurations provide a valuable opportunity to compare the predicted spectra at many points along the cavity ceiling and band-limited amplitude along the cavity length. We conclude that for such cavity flows, all DES models perform similarly well and are superior to unsteady RANS.

1.0 INTRODUCTION

The design of weapons bays for military aircraft applications uses a variety of design tools and methodologies. The initial design will typically employ simple, rapid, low cost empirical or semi-empirical prediction methods but these are generally unsuitable for more realistic and complex weapons bay configurations. Advanced modelling such as CFD offers the potential of higher fidelity, in particular of geometrically complicated weapons bay configurations including bulkheads, bay internals (pipe runs, cable trays and actuators), palliatives (ramps and spoilers) and complex store topologies, including launchers and multiple weapon fits.

Some success [1,2] has been reported in the use of URANS methods for modelling the narrowband Rossiter mode [3] components of the acoustic spectra. It is widely accepted that URANS methods are currently unable to predict the other contribution to the acoustic spectrum, namely the broadband. The literature [4-6] also shows the utilisation of more advanced turbulence modelling methodologies such as Detached Eddy Simulation [7] (DES) and Large Eddy Simulation (LES). The broadband spectra may have lower energy content than the narrowband (per unit frequency), but weapons bay structures, associated equipment and weapons will be continually exposed to significant fatigue damage from a wide range of frequencies. From a structural design viewpoint, to minimise damage, it is vital to avoid the possibility of a structural mode coinciding with a high energy Rossiter mode. Wind tunnel testing has shown the variability of Rossiter mode frequency with aircraft operating parameters such as Mach number. Consequently it is more desirable to design weapons bay structures to have modal frequencies outside the expected frequency range of Rossiter modes. Significant effort therefore is being invested in the prediction and amelioration of the broadband spectra through the development of affordable LES-type methodologies in design analysis.

Paper presented at the RTO AVT Symposium on "Functional and Mechanical Integration of Weapons and Land and Air Vehicles", held in Williamsburg, VA, USA, 7-9 June 2004, and published in RTO-MP-AVT-108.

In this paper, CFD calculations are performed on the M219 cavity [8] at Mach 0.85, and compared with experimental data from QinetiQ [9]. The cavity has a width/depth ratio of unity and a length/depth ratio of 5, and can be termed a 'deep' cavity because the separated shear layer at the leading edge does not attach to the weapons bay ceiling. Two cavity configurations are assessed. The first is referred to as 'doors-on' in which the bay doors are opened to 90º. The second 'doors-off' assembly is clear from the reference. The former exhibits narrowband, second Rossiter mode dominance, while the latter case the first three Rossiter modes are of similar magnitude and of a broadband type.

In the work presented here we qualify the partial success of URANS applied to unsteady cavity flow, but identify the regime in which its performance is uncertain. All DES variants are assessed, and are found consistently to perform better than URANS. LES is not considered because the requirement to resolve the boundary layer renders it impractical for the more complex industrial configurations described above.

2.0 CAVITY CONFIGURATIONS

The cavity's rectangular plan-form of 20×4in., shown in Figure 1, is cut into a flat plate 31in. from the rig's sharp leading edge and 1in. off-centre from the rig centreline. The inclined sides of the rig are not modelled. Only the flow inside cavity and below the flat plate is considered. Ten Kulite transducers (K20 closest to the cavity fore wall, consecutively numbered to K29 closest to the aft wall) were located on the cavity ceiling along the rig centreline, equally spaced between 1 and 19 inches from the front of the cavity. Two configurations are modelled, with and without bay doors.

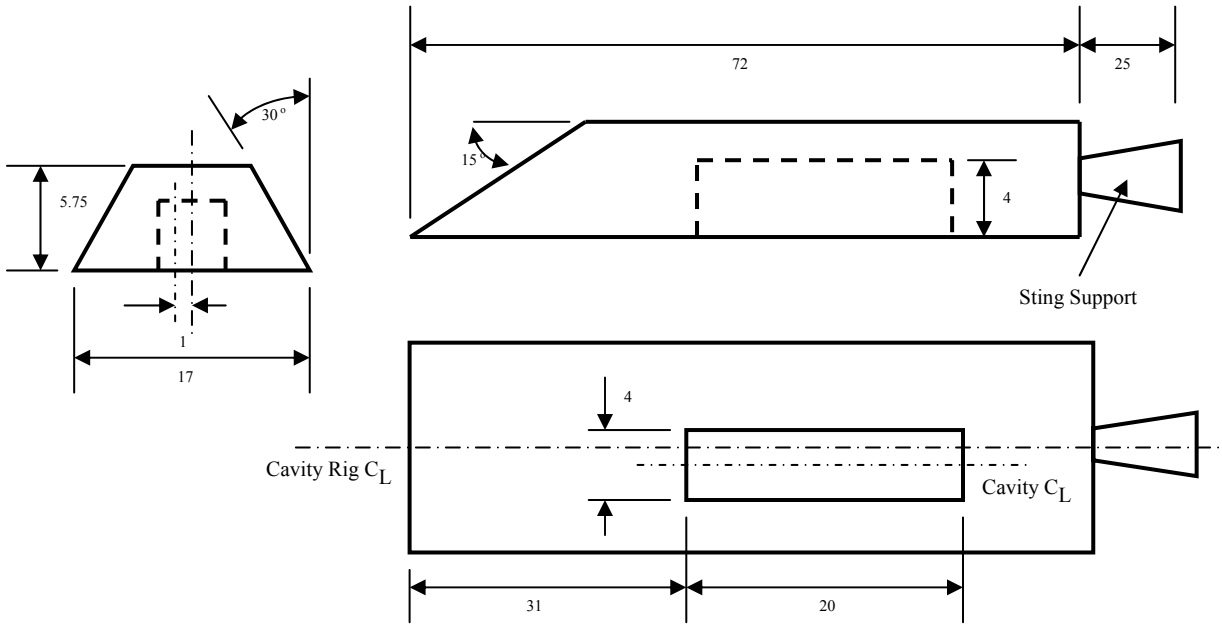

Figure 1: Experimental Rig of the M219 4in. Cavity Model (dimensions in inches)

3.0 COMPUTATIONAL MODEL

3.1 DES Turbulence Model Variants

All variants behave in such a way that the source terms dominate the transport equations for the turbulence variables in regions where the flow becomes detached and the turbulence is in equilibrium.

3.1.1 DES based on Spalart-Allmaras [7]

Equating the production and dissipation terms, we recover the same form as a Smagorinsky sub-grid scale viscosity,

$$\nu_t = \left(\frac{C_{b1}}{C_{\omega 1} f_\omega} \right) \Delta^2 S^{\frac{1}{2}} \tag{1}$$

If the length scale Δ is reinterpreted as the DES filter length based on a mesh dimension and pre-multiplier, $C_{DES/S-A}\Delta$, then $C_{DES/S-A}$ takes the value 0.65 according to the usual values for the Smagorinsky constant, C_s, and Spalart-Allmaras coefficients,

$$C_{DES/S-A} = \left(\frac{C_s C_{\omega 1} f_\omega}{C_{b1}} \right)^{\frac{1}{2}} \tag{2}$$

This is confirmed to be the appropriate value by numerical calibration tests — see section 3.3.

3.1.2 DES based on *k*-ω-SST

Travin [10] describes modifications necessary for Menter's *k*-ω-SST to behave as an LES sub-grid viscosity model. The length scales comes from

$$l_{k-\omega} = \frac{k^{\frac{1}{2}}}{\beta^* \omega} \tag{3}$$

The DES modified length scale then becomes

$$l_{DES/k-\omega} = \min\left(l_{k-\omega}, C_{DES/k-\omega}\Delta\right) \tag{4}$$

where $C_{DES/k-\omega}\Delta$ is the DES filter length. $C_{DES/k-\omega}$ takes the value 0.61, and the dissipation term in the ω-equation is written as;

$$D^k_{DES/k-\omega} = \frac{\rho k^{\frac{3}{2}}}{l_{DES/k-\omega}} \tag{5}$$

3.1.3 DES based on *k*-ε

Our own DES-variant [11] for *k*-ε follows identically.

The length scale comes from k and ε as follows;

$$l_{k-\varepsilon} = \frac{k^{\frac{3}{2}}}{\varepsilon} \tag{6}$$

The DES modified length scale then becomes

$$l_{DES/k-\varepsilon} = \min\left(l_{k-\varepsilon}, C_{DES/k-\varepsilon}\Delta\right) \tag{7}$$

where $C_{DES/k-\varepsilon}\Delta$ is the DES filter length and $C_{DES/k-\varepsilon}$ takes the value 0.73. This means that the dissipation term in the k-equation is written as;

$$D^{k}_{DES/k-\varepsilon} = \frac{\rho k^{\frac{3}{2}}}{l_{DES/k-\varepsilon}} \tag{8}$$

3.2 Mesh Structure

Trimmed cell meshing technology [12] was used to produce a grid containing approximately 1,100,000 predominantly perfect hexahedral cells, coarser in the free stream with successive 2×2 refinement approaching the separated shear layer and walls. Except near the doors, the doors-on and door-off meshes are identical. Figures 2 and 3 illustrate the longitudinal and transverse mesh distributions for the doors-on case.

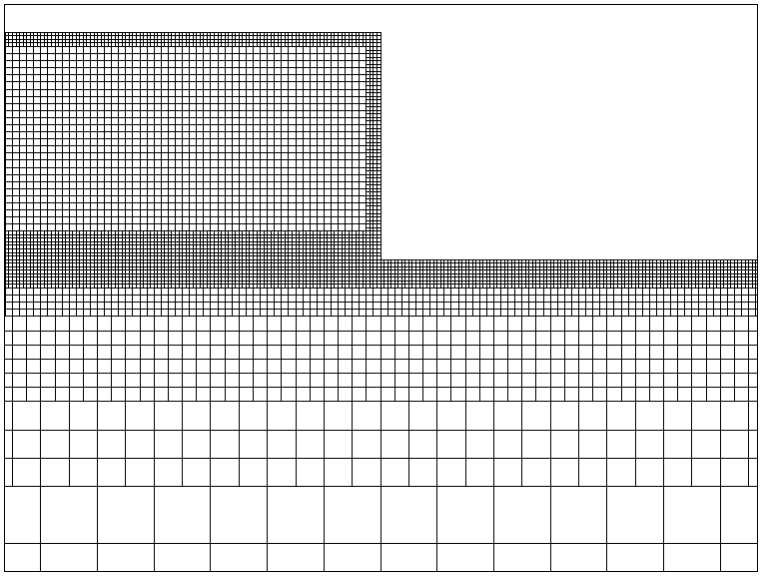

Figure 2: Longitudinal mesh distribution (aft wall detail)

The near-wall mesh spacing results in y^+ values of less than 300 everywhere, except very close to the attachment at the cavity aft wall. We recall that DES requires only RANS-type resolution in the near-wall region.

The computational domain extends 31 inches upstream of the cavity, corresponding to the sharp leading edge of the rig, at which free-stream momentum conditions are applied. A free-stream pressure boundary

is defined 21 inches downstream of the cavity aft wall. Boundaries to the side are placed 4 inches from the cavity side edges, and the bottom boundary 68 inches normal to the rig surface. These settings ensure that the flow inside the cavity is not affected by boundary interference.

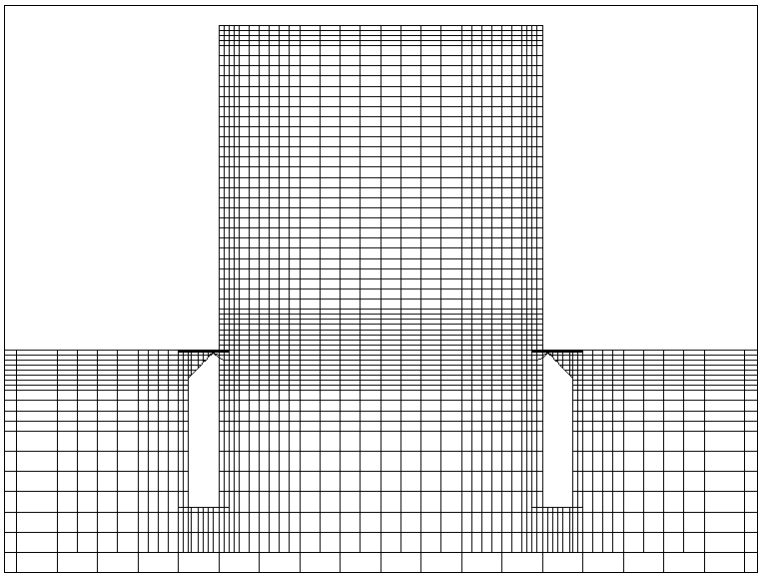

Figure 3: Transverse mesh distribution (detail of bay doors)

3.3 Discretisation

All calculations were performed using STAR-CD [13], which employs the PISO algorithm [14] for transient calculations. A time step advance of 2×10^{-5} seconds corresponds to mean convection Courant numbers of approximately 2, and local maximum Courant numbers below 10.

STAR-CD can be run using second-order upwind ('monotone advection and reconstruction scheme', MARS) or centred spatial schemes. The latter is preferred for LES. A standard numerical calibration test on decaying homogeneous isotropic turbulence allows for the setting of the sub-grid viscosity pre-multiplier. This calibration was performed for all the DES variants using a mesh of 64 [3]. In the case of the Spalart-Allmaras DES model. Figure 4 compares the measured energy spectrum from Comte-Bellot and Corrsin [15], to results from three combinations of discretisation scheme with or without sub-grid viscosity. The 'correct' behaviour achieved by the centred scheme is tuned by setting an appropriate value for C_{DES}, whilst the upwind scheme over-predicts the decay. An interesting result is that the upwind scheme without sub-grid scale viscosity exhibits artificial diffusion, which mimics the effect of the sub-grid scale viscosity.

This important result has consequences for DES. Following the suggestion of Travin [10], the solver employs advection scheme blending based on local vorticity and strain, hopefully to ensure that the centred scheme is used where the turbulence model is likely to be performing in LES mode, and upwinding elsewhere.

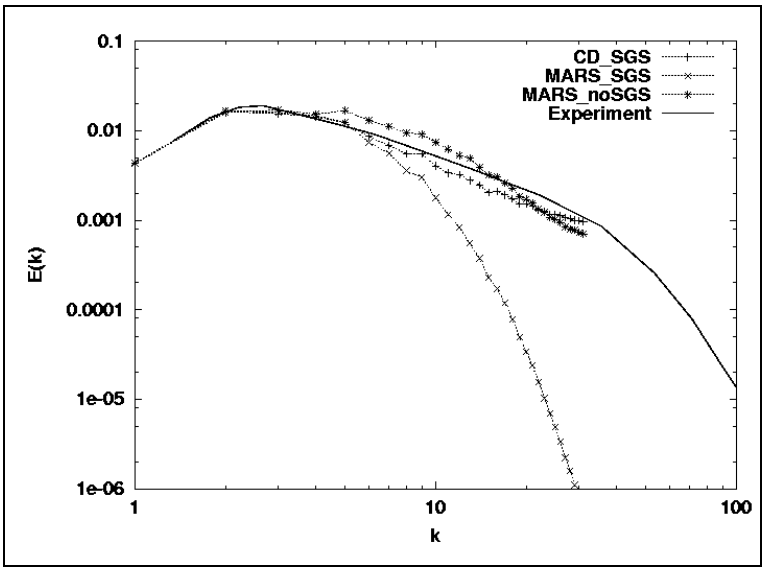

Figure 4: Homogeneous isotropic turbulence decay — comparison of advection discretisation schemes and effects of sub-grid scale viscosity

4.0 EXPERIMENTAL DATA

The unsteady pressure measurements are inherently noisy, as is apparent from Figure 5 for the tenth Kulite location (K29) at the downstream end of the cavity without bay doors. Smoothing is achieved by combining 34 windows of data, each of 0.1 seconds duration. The data are interpreted in the form of overall RMS pressures along the cavity ceiling and spectra at each of the ten Kulite positions.

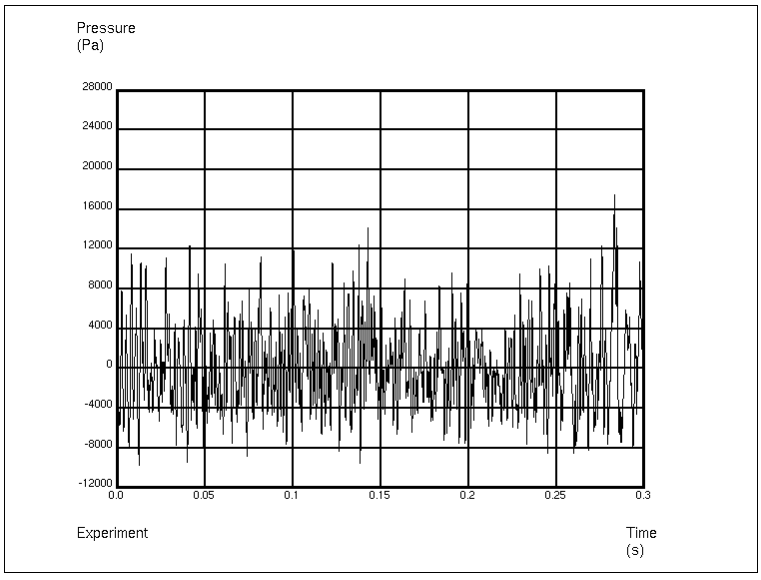

Figure 5: Experimental K29 pressure trace to 0.3 seconds

The door-on case exhibits second Rossiter mode dominance, a narrowband peak appearing at 380Hz for all ten Kulite measurement points. The first, third and fourth modes have much lower amplitudes and are broadband, peaking at approximately 170Hz, 590Hz and 760Hz respectively. In the doors-off case, maxima are observed at similar frequencies.

Band limited RMS pressures reveal in more detail the contribution from each Rossiter mode. Each modal band is decided from processing the Power Spectral Density, choosing frequencies that bracket the peak. The resulting P_{rms} curves are then observed to have unique mode-shapes identifying the mode;

- 1st mode; skewed 'V' shape, banded between 50-250Hz for both doors-on and off,
- 2nd mode; skewed 'W' shape, banded between 350-450Hz (doors-on) and 300-500Hz (doors-off),
- 3rd mode; skewed 'V-W' shape, banded between 500-700Hz for both doors-on and off,
- 4th mode; skewed 'W-W' shape, banded between 750-800Hz (doors-on) and 700-900Hz (doors-off).

5.0 SIMULATIONS

All transient calculations commenced from steady-state simulations run for 1000 iterations, and were advanced at a time-step increment of 20μs. An elapsed time of 0.5s (25,000 time-steps) takes approximately 5.5 days on eight 2.8GHz Intel Pentium 4 XEON processors under Linux. If we define the characteristic time to be that for the free stream to pass between the fore and aft edges, 0.5 seconds corresponds to just over 250 passes.

5.1 URANS vs. DES

We take for this datum comparison the URANS and DES models based on *k*-ε. There is a noticeable difference between the instantaneous *k*-ε (URANS) and DES/*k*-ε flow-fields. Figure 6, taken at 0.3 seconds after the steady-state restart, demonstrates that DES captures more chaotic flow structures. This is consistent with large eddy simulation and indicates broadband flow excitations, confirmed by the predicted pressure traces at Kulite K29 for the doors-off case.

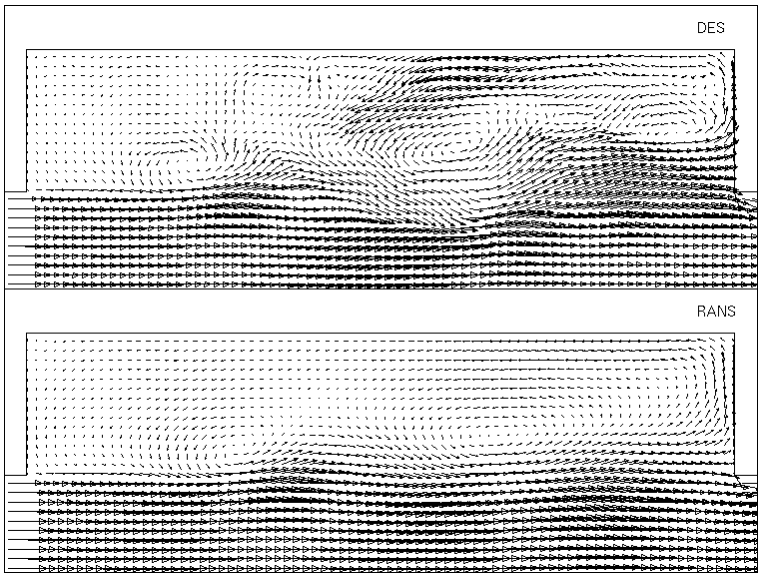

Figure 6: Symmetry plane snapshot at t = 0.3sec; DES/*k*-ε (top) and URANS/*k*-ε (bottom)

Figures 7 and 8, for DES/*k*-ε and URANS/ *k*-ε respectively, show that the K29 trace is noisy in the case of the former, as with the experiment (Figure 5), but regular and limit-cycled in the latter case.

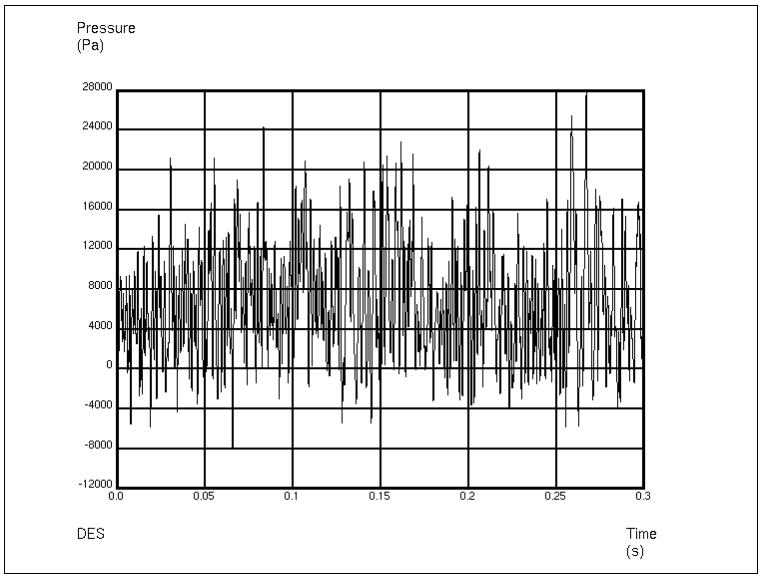

Figure 7: DES K29 pressure trace to 0.3 seconds, *doors-off*

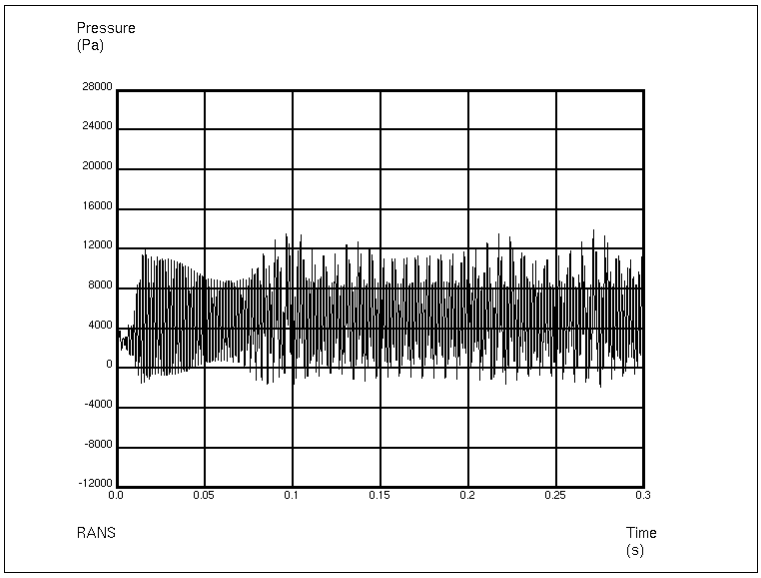

Figure 8: URANS/*k-ε* K29 pressure trace to 0.3 seconds, *doors-off*

Data processing of the URANS/*k*-ε result is made simple due to its limit-cycled nature. Calculations were only run to 0.3 seconds, and the final 0.1 seconds processed. For DES, we chose to run for 0.5 seconds and to process the last 0.2 seconds in 3 overlapping windows, therefore also giving a 0.1 second or 10Hz resolution. (In Section 5.2, the effect of processing different time samples is assessed.)

5.1.1 Doors-on configuration

Figure 9 shows RMS pressures, overall and band-limited, for URANS/*k*-ε and DES/*k*-ε compared with experiment.

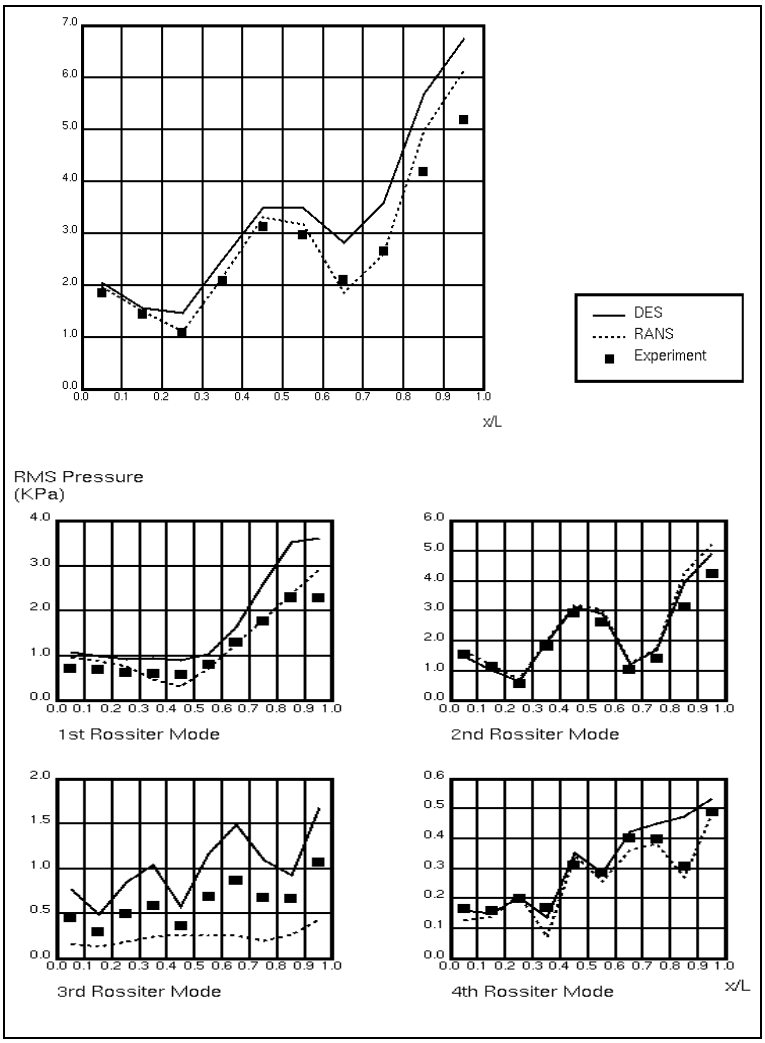

Figure 9: Overall (top) and band limited (bottom) P_{rms} along the cavity ceiling, *doors-on*

Both DES and unsteady RANS are shown to capture the dominant second Rossiter mode extremely well, with only a small over-prediction apparent at the downstream end. This mode is known to be due to the streamwise convection of vortices shed from the cavity fore edge.

The first mode is less dominant. URANS/k-ε predicts the level and shape very well. DES over-predicts the level but captures shape well. Similarly, the DES shape for the third Rossiter mode is well captured but the level is over-predicted. The URANS signal is poor. The fourth mode is the weakest, but both turbulence models predict the level and shape very well. We can conclude from the overall and band limited RMS pressures that URANS is accurate on the first, second and fourth modes. DES captures all mode shapes very well, but over-predicts the first and third modes.

More detail emerges when looking at point spectra. Figure 10 show the Power Spectral Density against frequency for all ten Kulite locations K20 to K29. PSDs are plotted on a log scale to accentuate the broadband contribution. The main difference between URANS and DES is clearly seen to be that URANS fails to predict the background broadband contribution, and that DES does so well.

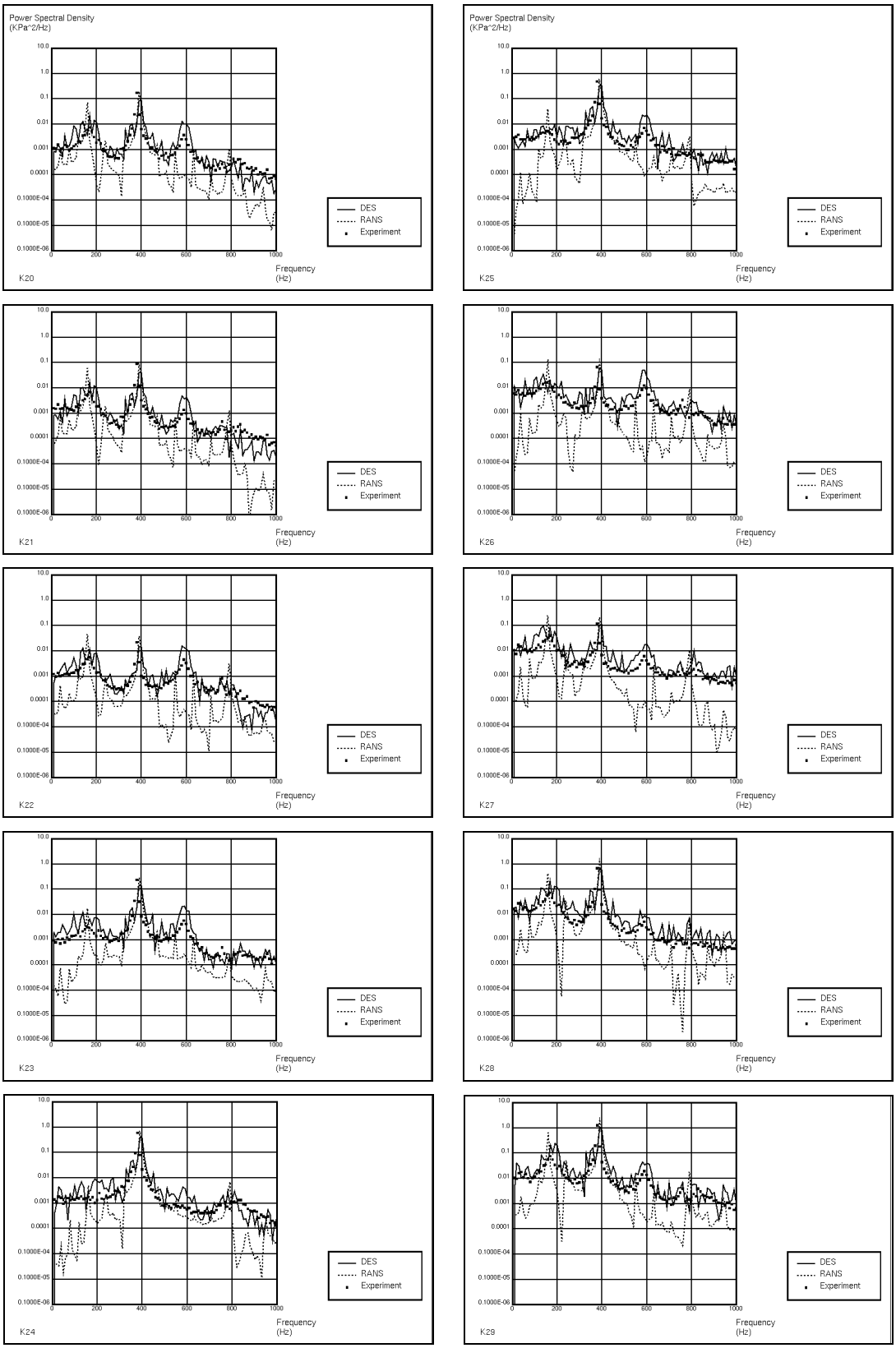

Figure 10: PSD for all ten Kulite locations, *doors-on*

All ten Kulite measurements register the four Rossiter modes to varying levels of accuracy. The second is always present as narrowbanded and dominant. URANS performs consistently well, except that the first, third and fourth modes appear as narrowband peaks. DES does better in capturing the second mode at all locations and more faithfully represents the others as broadband modes.

Finally, to summarize findings for the doors-on case, URANS produces good predictions of RMS pressure variation along the cavity ceiling and the main narrowband second mode, but DES is superior in every detail, particularly in its ability to capture the broadband.

5.1.2 Doors-off configuration

In the doors-off configuration, the cavity shear layer is no longer constrained in the transverse direction by the presence of bay doors. This introduces greater three-dimensionality to the flow behaviour inside the cavity, which has the effect of accentuating the first and third modes and suppressing the second mode.

Figure 11, showing overall and band limited RMS pressures for the doors-off case, should be compared directly with Figure 9 for the doors-on configuration. The first, second and third modes are now all of approximately equal magnitude.

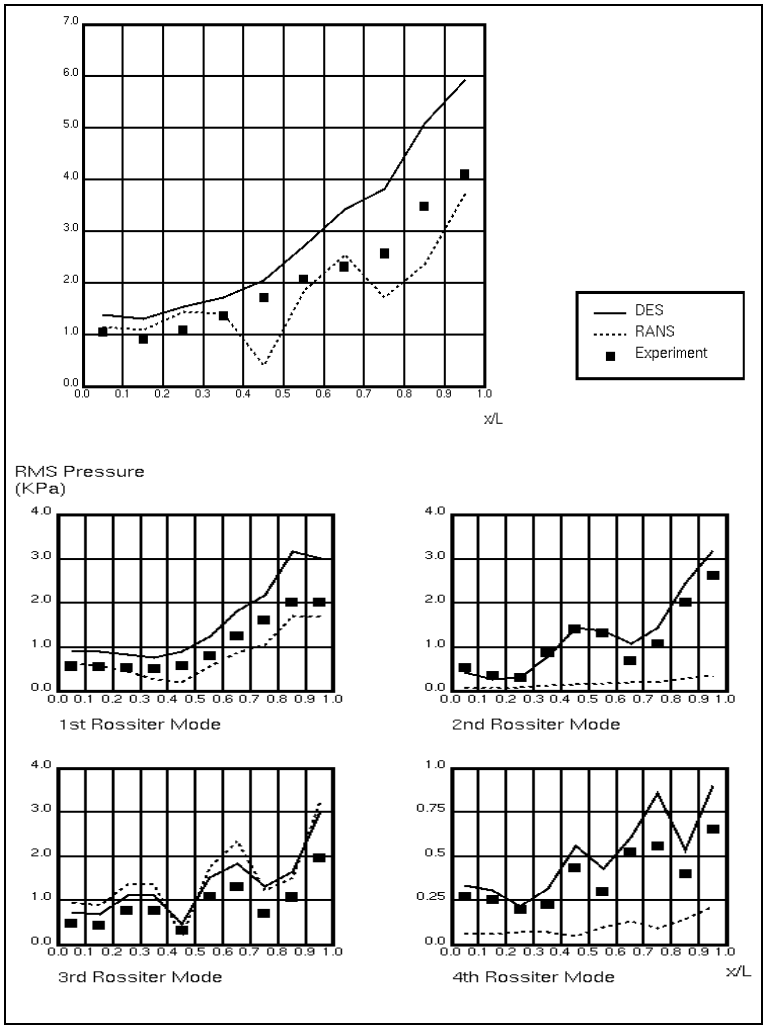

Figure 11: Overall and band limited P_{rms} along cavity centre-line, *doors-off*

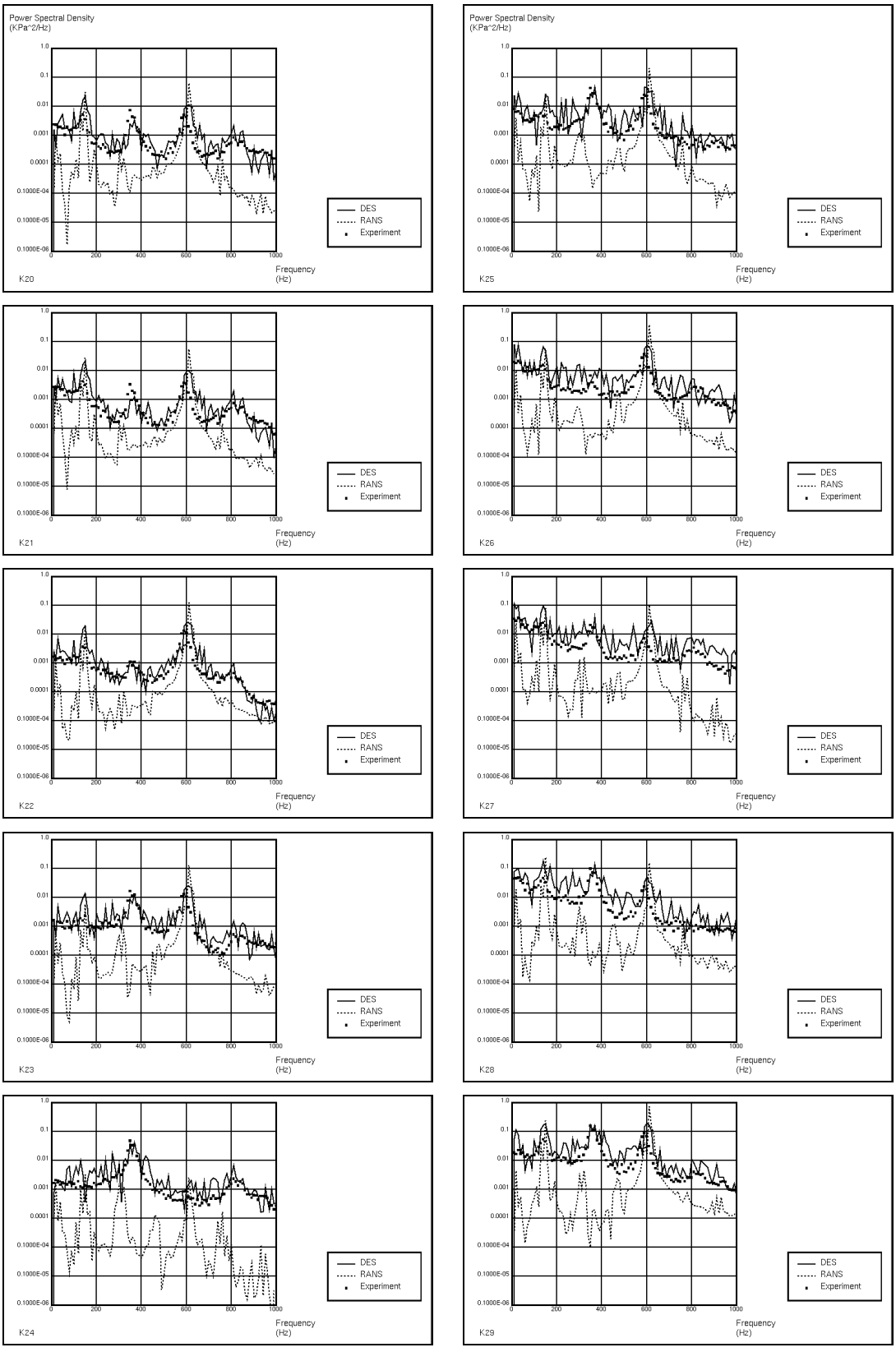

Figure 12: PSD for all ten Kulite locations, *doors-off*

The unsteady RANS model performs poorly, with overall RMS pressure variation along the cavity ceiling indicating third mode dominance. The first mode is under-predicted. The second and fourth modes are grossly under-predicted.

DES performs more consistently. As in the doors-on case, the second mode is modeled extremely well. The first, third and fourth mode shapes are captured accurately, but levels over-predicted, which leads to an overall over-prediction of RMS pressure.

Turning attention to the spectra at the ten Kulite locations, Figure 12 demonstrates the advantage of DES/*k*-ε over URANS/*k*-ε. The background broadband noise is well predicted by DES. All four modes are captured, as are the relative peak magnitudes between the modes at all the points along the cavity ceiling.

By contrast, URANS under-predicts the background broadband contribution by at least one order of magnitude. At Kulite location K24, URANS fails to capture the second and fourth modes, incorrectly exaggerates the first and third modes, and under-predicts the background broadband contribution by more than two orders.

We recall that the pressure-time history for Kulite K29 in Figure 8 shows a transition from one limit-cycled oscillation containing a single sinusoidal narrowband mode to a second containing a superposition of two sinusoids. The earlier part corresponds with the third Rossiter mode only, and the latter part with the first and third modes superimposed, as we can see from Figure 12. These facts indicate the model's general unsuitability.

5.2 Data Sampling Effects

The experimental pressure traces taken for a total of 3.4 seconds are inherently noisy.

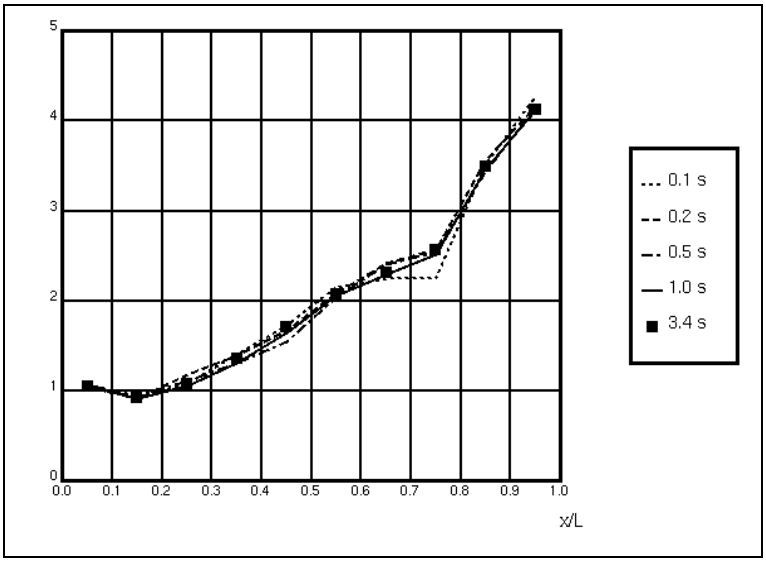

Figure 13: Sampling effects on overall P_{rms} (KPa) along the cavity ceiling; experimental data

Smooth P_{rms} and pressure spectra are achieved by combining 34 windows of data, each of 0.1 seconds duration. Since it is neither practical nor desirable to run computations for the same time span, we choose first to assess the effects of using a smaller number of 0.1 second time-windows from the experimental pressure traces, and then to assess the effects of different time-windows from the DES simulation.

Figure 13 shows that at least 1.0 second of the experimental data must be processed to obtain a result that is equivalent to the 3.4 seconds sample.

Conversely, Figure 14 shows the P_{rms} curves for the DES result over a range of sample periods from 0.1 to 0.5 seconds, averaged in the same manner as the experimental data but with the first 0.1 seconds discarded to eliminate start-up effects. This shows that at least a 0.4 second sample is required to obtain a negligible level of deviation between sample windows.

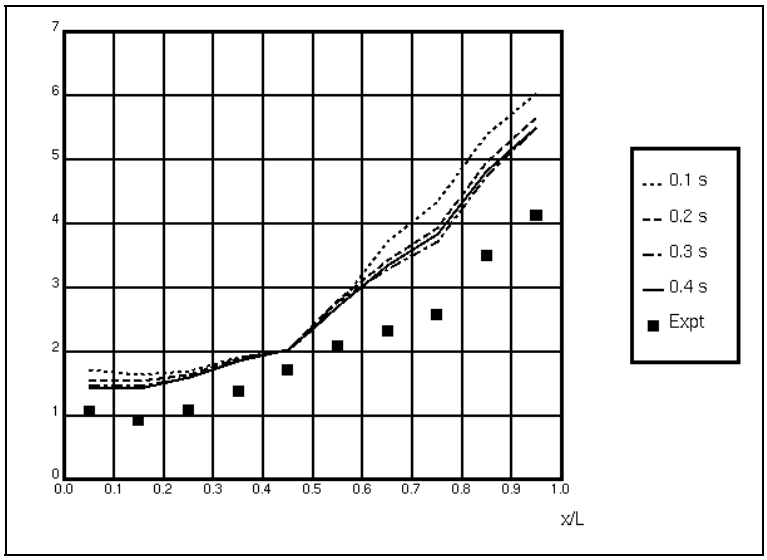

Figure 14: Sampling effects on overall P_{rms} (KPa) along the cavity ceiling; DES data

Therefore, it is recommended that DES runs should provide data equivalent to an elapsed time of 0.5 seconds, allowing the initial 0.1 seconds to be discarded and the remaining 0.4 seconds to be processed. Shorter samples should be interpreted with care.

5.3 DES Turbulence Model Variants

Figures 15 and 16 provide a comparison of the three DES variants, showing overall and band-limited RMS pressure and acoustic spectra for the doors-off case at Kulite position K29 on the cavity ceiling (which is typical of the results at all other Kulite locations). DES performs consistently, with all four mode shapes captured accurately.

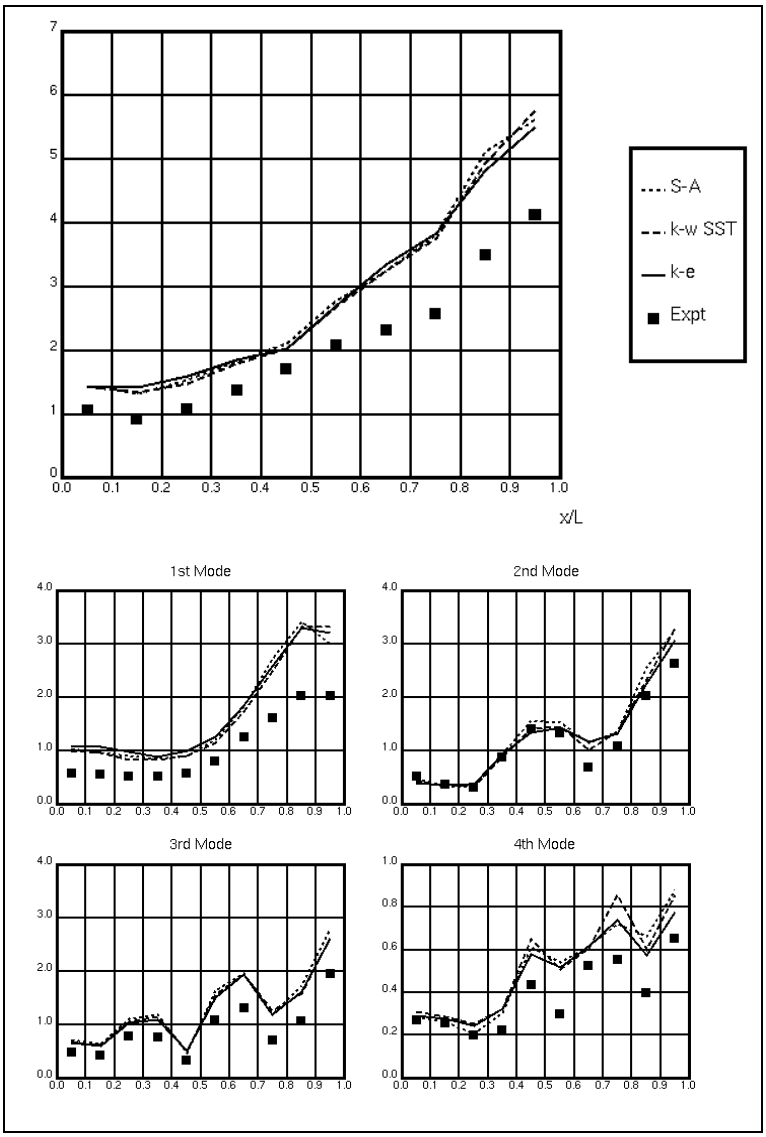

Figure 15: Overall and band-limited P_{rms} (KPa) along the cavity ceiling for DES variants

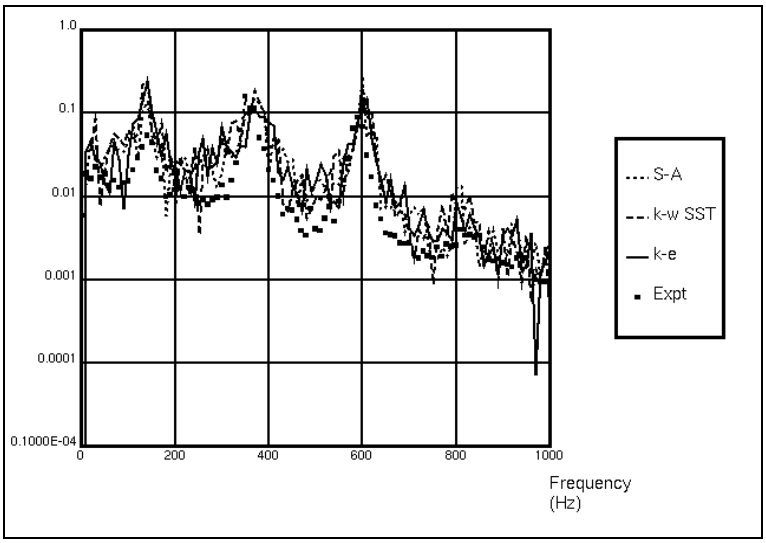

Figure 16: PSD (KPa^2/Hz) at Kulite location K29 for DES model variants

No major differences were observed between the DES variants. For this application, such a result is clearly desirable, demonstrating that the flow is dominated by large-eddy structures and that the modelling parameters were properly chosen and calibrations correctly performed.

6.0 CONCLUSIONS

We have demonstrated the value of DES turbulence modelling for the M219 cavity, L/D = 5 at Mach 0.85, compared its relative merits against the equivalent RANS based approach, and established the superiority of the former when compared to detailed experimental data. We have observed consistent Rossiter mode shape predictions, only slightly over-predicting RMS pressure and Power Spectral Densities. Eliminating the over-predictions will be one focus for future work.

For this cavity configuration, we recommend that a minimum of 0.5 seconds should be simulated, allowing for startup effects to be neglected and a full 0.4 seconds of simulation data to be processed.

All DES variants, namely Spalart-Allmaras, *k*-ε and *k*-ω-*SST*, produce broadly similar results that match the measurements well, indicating that the flow is dominated by large eddy structures and that the chosen combination of numerical parameters are appropriate.

8.0 REFERENCES

[1] Henderson, J., Babcock, K., and Richards B.E. 2000. Subsonic and transonic transitional cavity flows, 6th AIAA/CEAS Aeroacoustics Conference and Exhibit, Paper No. AIAA-2000-1966, June 2000.

[2] Inagaki, M., Murata, O., Kondoh, T., and Abe, K. 2002. Numerical prediction of fluid-resonant oscillation at low Mach number, *AIAA Journal*, Vol. 40, No. 9, pp. 1823-1908, September 2002.Rossiter, J.E. 1964. Wind tunnel experiments on the flow over rectangular cavities at subsonic and transonic speeds, Aeronautical Research Council, Reports and Memoranda 3438, London, 1964.

[4] Shieh, C.M., and Morris, P.J. 2000. Parallel computational aeroacoustic simulation of turbulent subsonic cavity flow, 6th AIAA/CEAS Aeroacoustics Conference and Exhibit, Paper No. AIAA-2000-1914, June 2000.

[5] Rizzetta, D.P., and Miguel, R.V. 2002. Large eddy simulation of supersonic cavity flowfields including flow control, 8th AIAA/CEAS Aeroacoustics Conference and Exhibit, Paper No. AIAA-2002-2853, June 2002.

[6] Mendonça, F., Allen, R., de Charentenay, J., and Lewis, M. 2002. Towards understanding LES and DES for industrial aeroacoustics predictions, International Workshop on LES for Acoustics, DLR Göttingen, Germany, 7-8 October 2002.

[7] Spalart, P.R., Jou, W.H., Strelets, M., and Allmaras, S.R. 1997. Comments on the feasibility of LES for wings, and on a hybrid RANS/LES approach, First AFOSR International Conference on DNA/LES, Ruston, Louisiana, USA.

[8] Henshaw, M.J. de C. 2000. M219 cavity case in verification and validation data for computational unsteady aerodynamics, RTO-TR-26, AC/323(AVT)TP/19, October 2000.

[9] Ross, J.A. Private communications, QinetiQ, Bedford, MK41 6AE, UK.

[10] Travin, A., Shur, M., Strelets, M., and Spalart, P. 2002. Physical and numerical upgrades in the detached-eddy simulation of complex turbulent flows, *in* "Advances in LES of Complex Flows" (Eds. P. Friedrich and W. Rodi), pp. 239-254, Kluwer Academic Publishers.

[11] Mendonça, F., Allen, R., de Charentenay, J., and Kirkham, D. 2003. CFD prediction of narrowband and broadband cavity acoustics at M = 0.85, 9th AIAA/CEAS Aeroacoustics Conference and Exhibit, Paper No. AIAA-2003-3033, May 2003.

[12] The *pro-am* User Manual, January 2003, adapco, New York.

[13] STAR-CD Version 3.15, User Guide and Methodology Manuals, 2001, Computational Dynamics Limited, London, UK.

[14] Issa, R.I., Gosman, A.D., and Watkins, A.P. 1986. The computation of compressible and incompressible recirculating flows by a non-iterative implicit scheme, *J. Comp. Phys.*, No. 62, pp. 66-82.

[15] Comte-Bellot, G., and Corrsin, S. 1971. Simple Eulerian time-correlation of full- and narrow-band velocity signals in grid-generated 'isotropic' turbulence, J. Fluid Mech., Vol. 48, No. 2, pp. 273-337.

DISCUSSION EDITING

Paper No. 22: RANS and DES Turbulence Model Predictions on the M219 Cavity at M = 0.85

Authors: Richard Allen, David Kirkham

Speaker: Fred Mendonça.

Discussor: M. Tutty

Question: Given you believe that technique is applicable to structures. How many years away, do you feel that techniques will be available to predict electronics in weapons fatigue life.

Speaker's Reply: Difficult to answer specifically since I am not familiar with the full flow Reynolds number range experienced in cavity release envelope, but it is possible to obtain high resolution predictions (LES based) up to reynolds numbers of 1*10^6 (computations of approx 1 month on modern clusters) today.

Discussor: G. W. Foster

Question: How do the run time & memory requirements for the various DES (K-E, Spalart Almaras Imans, etc.) compare, and how do they compare with URANS?

Speaker's Reply: Most of the solver-work is done by the STAR-CD pressure-velocity part. Therefore the DES variants only differ by a few per cent (less than 5%) The same applies to DES compared with its URANS equivalent

Discussor: M. Khalid

Question: Since you use wall function approach for boundary condition at the wall, are you not likely to overlook some physics especially when you have separated flows?

Speaker's Reply: The wall boundary conditions is hybrid by nature, incorposating wall-functions if the near-wall cell is in the fully turbulent part of the boundary layer; but also incorporates formulations applicable for the laminar and viscous sublayers. This makes the wall treatment independent of y+ in the lower range (0 < y+ < 300 approx.)#

Discussor: A. Cenko

Question: If polyhedrals are so much better than tetraherals, why doesn´t everyone use them?

Speaker's Reply: Everyone should, and perhaps will (for complex geometries) before long. Only very recently do we have access to robust polyhdra mesh generators, and CFD solvers capable of handling arbitrary polyhedra. The STAR-CD family seems to be the only widespread embodiment of both, at present.